Physics in Medicine & Biology

On the relativistic impulse approximation for the calculation of Compton scattering cross sections and photon interaction coefficients used in kV dosimetry

To cite this article before publication: Xiaoya Judy Wang *et al* 2020 *Phys. Med. Biol.* in press https://doi.org/10.1088/1361-6560/ab8108

On the relativistic impulse approximation for the calculation of Compton scattering cross sections and photon interaction coefficients used in kV dosimetry

Xiaoya Judy Wang[1], Beatriz Miguel[2], Jan Seuntjens[1], and José M Fernández-Varea[3,1]

[1]Department of Physics & Medical Physics Unit, McGill University. Montréal, Québec H3A 2T8, Canada

[2]Departamento de Ingeniería Química y Ambiental, Universidad Politécnica de Cartagena. Paseo Alfonso XIII 52, ES-30203 Cartagena, Spain

[3]Facultat de Física (FQA & ICC), Universitat de Barcelona. Diagonal 645, ES-08028 Barcelona, Catalonia, Spain

Abstract.

We calculate differential and integrated cross sections for the Compton interaction as well as mass attenuation (μ^{C}/ρ), mass energy-transfer ($\mu^{\mathrm{C}}_{\mathrm{tr}}/\rho$), and mass energy-absorption (μ_{en}/ρ) coefficients, within the relativistic impulse approximation (RIA) using Compton profiles (CPs) obtained from unrestricted Hartree–Fock electron densities. We investigate the impact of using molecular as opposed to atomic CPs on dosimetric photon interaction coefficients for air, water and graphite, and compare our cross sections to the simpler Waller–Hartree (WH) and Klein–Nishina (KN) formalisms. We find that differences in μ^{C}/ρ and $\mu^{\mathrm{C}}_{\mathrm{tr}}/\rho$ resulting from the choice of CPs within the RIA are small relative to the differences between the RIA, WH, and KN calculations. Surprisingly, although the WH binding corrections seem accurate when considering μ^{C}/ρ, there are significant discrepancies between the WH and RIA results when we look at $\mu^{\mathrm{C}}_{\mathrm{tr}}/\rho$. The WH theory can differ substantially from the predictions of KN and the RIA in the tens of keV range (e.g., 6–10% at 20 keV), when Compton scattering becomes the dominant interaction mechanism. For lower energies, the disagreement further grows to about one order of magnitude at 1 keV. However, since the photoelectric effect transfers more energy than the Compton interaction in the tens of keV range and below, the differences in the total μ_{en}/ρ values resulting from the choice of Compton models (KN, WH, or RIA) are not larger than 0.4%, and the differences between WH and the other two theories are no longer prominent.

1. Introduction

Photon interaction data and electron stopping powers form the basis of most dosimetric standards and radiation interaction applications in medical physics, both for therapy and for imaging. In radiation dosimetry these data play a crucial role in the conversion of detector readings to absorbed dose either through cavity theory or via Monte Carlo (MC) radiation transport calculations (Büermann & Burns (2009), Burns & Büermann (2009)), and as such these data affect primary radiation standards. More clinically-oriented applications include backscatter factors and mass energy-absorption coefficient ratios used in kV dosimetry protocols for radiotherapy and radiobiology and in diagnostic radiology applications (Benmakhlouf et al. (2011), Andreo (2019), Hill et al. (2014)) as well as in x-ray fluorescence calculations and measurements (O'Meara et al. (1998)). Another area of application where the actual Compton angular distribution is critical is x-ray imaging of scattered photons for the characterization of biological samples in which Compton differential cross sections (DCSs) are needed for modelling the backscatter distribution (Johns (2002)). Compton DCSs also play a key role in the determination of photon energy distributions produced by x-ray tubes from spectra acquired with a Compton spectrometer. The early developments of this technique were reviewed by Alm Carlsson and her co-workers (Alm Carlsson et al. (1989)). A state-of the-art implementation has been described e.g. in (Terini et al. (2020)).

For photons, mass attenuation coefficients and mass energy-absorption coefficients are most often based on the tabulations by Berger & Hubbell (1987), Seltzer (1993), and Hubbell & Seltzer (1995). Other photon data include the commonly-used EPDL'97 (Cullen et al. (1989, 1997)) and the older Storm & Israel (1970) data sets. A recent publication by Andreo and his co-workers aimed to establish an envelope of uncertainty for mass energy-absorption coefficients, but focused on the photoelectric cross sections (Andreo et al. (2012)). Here we study the uncertainties introduced by using different theoretical formalisms and their inputs for the Compton interaction in the low- to intermediate-energy range of 1 keV to 1 MeV. While μ^{C}/ρ has been tabulated in ICRU Report 90 (The International Commission on Radiation Units and Measurements (2016)) for the same models, a systematic comparison for $\mu^{\mathrm{C}}_{\mathrm{tr}}/\rho$ has not been made, and the effect on the total μ_{en}/ρ has not been reported.

The simplest approach for calculating incoherent scattering cross sections is the Klein–Nishina (KN) DCS, in which the photon is assumed to be scattered by a free electron at rest (Klein & Nishina (1929), Jauch & Rohrlich (1976)). As an improvement on KN, a well-known and frequently-used approximation is the Waller–Hartree (WH) theory (Waller & Hartree (1929)) which accounts for binding effects approximately through the incoherent scattering function (Hubbell et al. (1975, 1977)), but which neglects the spread in energy of photons scattered at a given angle (Doppler broadening) (Hubbell & Seltzer (1995), Hubbell (2006)). An important source of photon interaction data is from Seltzer (1993), who derived mass energy-absorption coefficients for elements and compounds using the WH model.

On the other hand, the most sophisticated method for calculating Compton scattering

cross sections is the S-matrix formalism (Bergstrom Jr et al. (1993), Bergstrom Jr & Pratt (1997), Pratt et al. (2010)). While the KN formula is derived within quantum electrodynamics (QED) assuming a free electron, the full S-matrix treatment consists of QED calculations in an external electromagnetic field (also called the Furry or bound-state interaction picture), which increases the complexity of the mathematical procedures. This theory represents the most accurate understanding of fundamental physics, although it is not suitable for tabulation of data for widespread implementation for all elements and covering the entire energy range of interest. In addition to the main Compton peak in the doubly differential cross section (DDCS), it predicts infrared divergences in the limit of low scattered photon energies due to the presence of any number of undetectable low-energy photons (Jauch & Rohrlich (1976)), and these divergences need to be cancelled out by considering the photoelectric DCS (McEnnan & Gavrila (1977), Botto & Gavrila (1982)). S-matrix calculations also deal with resonances which occur when scattered photon energies correspond to atomic fluorescence lines, and poles appear in the amplitude of one of the diagrams (Bergstrom Jr et al. (1993), Bergstrom Jr & Pratt (1997)).

Owing to the difficulties described above, the relativistic impulse approximation (RIA) has been the model which has been implemented in the MC codes PENELOPE (Salvat (2019)) and EGSnrc (Rogers et al. (2003)). The RIA incorporates both binding effects and Doppler broadening and yields an expression for the DDCS differential in the outgoing photon angle and energy (Ribberfors (1975), Ribberfors & Berggren (1982)). Accounting for the Doppler broadening has been shown to lead to corrections in mass energy-absorption coefficients of up to a few percent for low-Z materials of dosimetric interest (Ribberfors & Alm Carlsson (1985)). The key ingredient to the calculation of the RIA cross sections is the Compton profile (CP) of each atomic or molecular orbital, which is computed from the corresponding linear momentum distribution. Photon interaction coefficients for compounds used in dosimetry are modeled by adopting an independent-atom approach (Rao et al. (2004), Stutz (2014)), with the atomic CPs typically taken from the classical tabulation of Biggs et al. (1975).

Extensive comparisons of RIA with S-matrix theory have been discussed in (Bergstrom Jr et al. (1993)), where excellent agreement was found in the main Compton peak region of the DDCS when the incident energy and the energy transfer are large compared to the binding energy. Comparisons of DCSs are difficult since the RIA does not account for infrared divergences or resonances, and the S-matrix results can vary depending on the low-energy cutoffs applied to the integration of the DDCSs (Bergstrom Jr et al. (1993)). However, given the low-Z materials and energy interval considered in this work, the additional features predicted by the S-matrix theory are not expected to play a significant role, and we are well within the range where there is good agreement between the RIA and the S-matrix theory.

In this article we investigated for three materials of dosimetric interest (air, water, and graphite) the impact of using more realistic CPs on the Compton cross sections and interaction coefficients derived within the RIA, in the low- and intermediate-energy interval of 1 keV to 1 MeV. By also looking at DCSs, we discuss the differences between the RIA

and the WH approach to modelling binding effects, and highlight the limitations of the WH theory. Finally, we calculate the effect of using different Compton models on the total mass energy-absorption coefficient, including the photoelectric effect.

2. Background

In this section we give an overview of the three theoretical frameworks for Compton scattering considered in the present work, namely KN, WH, and RIA. We then briefly describe the unrestricted Hartree–Fock formalism from which we calculated the electron densities in momentum space and the CPs, and finally we review the basic definitions of photon interaction coefficients. We note that all the DDCSs and DCSs we calculate are independent of the azimuthal scattering angle ϕ because we only consider unpolarized photon beams.

2.1. Klein–Nishina approximation

A consistent theory for Compton scattering, in which a photon is scattered inelastically by an electron, requires a quantized description of the radiation field. In classical electrodynamics and at non-relativistic energies, Thomson scattering predicts no change in the scattered photon's wavelength and the collision is thus elastic. High-energy modifications to Thomson can describe light accelerating an electron to relativistic speeds, leading to a recoil of the electron and an associated Doppler shift of the scattered light, however this effect becomes arbitrarily small at low light intensities. Therefore, classical electrodynamics cannot explain general Compton phenomena, and quantization of the electromagnetic field is required.

In QED, the interaction between a photon and an electron is expressed as a perturbative series expansion, where each higher-order term is represented by a Feynman diagram having an additional vertex. Higher-order terms are called radiative corrections since they involve more virtual photons which mediate the interactions between vertices. After further assuming that the electron is free and at rest, the cross section calculated from the lowest-order term results in the well-known KN formula for the DCS per electron

$$\left(\frac{\mathrm{d}\sigma}{\mathrm{d}\Omega}\right)_{\mathrm{KN}} = \frac{r_\mathrm{e}^2}{2}\left(\frac{E'}{E}\right)^2\left(\frac{E'}{E}+\frac{E}{E'}-\sin^2\theta\right). \tag{1}$$

In the above, $r_\mathrm{e} \equiv e^2/m_\mathrm{e}c^2$ is the classical electron radius (e is the elementary charge, m_e is the electron rest mass, c is the speed of light in vacuum) whereas E and E' are, respectively, the initial and final photon energies, which are related to the polar scattering angle θ by the famous Compton relation

$$E' = E_\mathrm{C} \equiv \frac{E}{1+\frac{E}{m_\mathrm{e}c^2}(1-\cos\theta)}. \tag{2}$$

When the incoming photon energy is much higher than the electron's kinetic and binding energies, the assumptions made in the KN model are approximately valid, and the KN DCS is expected to be realistic. The atomic DCS is obtained by simply multiplying the one-electron DCS of Eq. (1) with the atomic number Z.

2.2. Waller–Hartree approximation

The simplest model for Compton scattering off of bound atomic electrons is known as the Waller–Hartree (WH) approximation, in which binding effects are incorporated by multiplying the KN DCS with the incoherent scattering function $S(q, Z)$ (Hubbell et al. (1975, 1977)), leading to the following atomic DCS‡

$$\left(\frac{\mathrm{d}\sigma}{\mathrm{d}\Omega}\right)_{\mathrm{WH}} = \left(\frac{\mathrm{d}\sigma}{\mathrm{d}\Omega}\right)_{\mathrm{T}} S(q, Z).$$

$$\left(\frac{\mathrm{d}\sigma}{\mathrm{d}\Omega}\right)_{\mathrm{WH}} = \left(\frac{\mathrm{d}\sigma}{\mathrm{d}\Omega}\right)_{\mathrm{KN}} S(q, Z) \tag{3}$$

with

$$S(q, Z) = \sum_{\epsilon>0} \left| \left\langle \epsilon \left| \sum_{j=1}^{Z} \mathrm{e}^{\mathrm{i}\mathbf{q}\cdot\mathbf{r}_j/\hbar} \right| 0 \right\rangle \right|^2, \tag{4}$$

where $\mathbf{r}_j$ is the position of the j-th atomic electron, $\mathbf{q} = \mathbf{k} - \mathbf{k}'$ is the momentum transfer vector, being $\mathbf{k}$ and $\mathbf{k}'$ the initial and final photon linear momenta, and q is its magnitude

$$q = \frac{1}{c}\sqrt{E^2 + E'^2 - 2EE'\cos\theta}. \tag{5}$$

$|0\rangle$ denotes the ground state of the atom, and $|\epsilon\rangle$ denotes an excited (bound) or ionized (free) state. Adding and subtracting the contribution of the ground state to the right-hand side of Eq. (4) and invoking the completeness of atomic states, the incoherent scattering function can be expressed in terms of only the ground-state wave function (Hubbell et al. (1975, 1977))

$$S(q, Z) = \left\langle 0 \left| \sum_{i=1}^{Z} \sum_{j=1}^{Z} \mathrm{e}^{\mathrm{i}\mathbf{q}\cdot(\mathbf{r}_i - \mathbf{r}_j)/\hbar} \right| 0 \right\rangle - \left\langle 0 \left| \sum_{j=1}^{Z} \mathrm{e}^{\mathrm{i}\mathbf{q}\cdot\mathbf{r}_j/\hbar} \right| 0 \right\rangle^2. \tag{6}$$

The second term is the square of the atomic form factor, which the reader may recognize from the atomic DCS for Rayleigh (i.e. elastic) scattering of photons.

The incoherent scattering function increases monotonically from zero at low momentum transfers to Z at high momentum transfers, at which point the WH and KN approximations are in agreement. Hubbell (1997) summarized the information prior to 1997 on the validity of the WH theory.

2.3. Relativistic impulse approximation

In general terms, the impulse approximation can be useful whenever a scattering problem involves a composite target consisting of many particles bound together. At its core, the impulse approximation relies on the assumption that the interaction time is short enough

‡ Eq. (3) results from the *ad hoc* replacement of the Thomson DCS with the KN DCS in the DCS for incoherent scattering derived within non-relativistic quantum mechanics,

that the state of the target does not change, i.e. any dynamics caused by binding forces can be neglected, and the full target potential only serves to create a momentum distribution for the bound particles. An accompanying assumption is typically made, namely that the scattered projectile only interacts with one of the particles in the target, and that this interaction does not involve the rest of the spectator particles. More specifically, the assumptions of the impulse approximation break down when the energy transfer is not much larger than the binding energy, which is most important for low incident energies and at small scattering angles. One could define a critical scattering angle θ^* or a critical incident energy E^* below which the impulse approximation might be expected to fail (Stutz (2014)), and indeed this was formulated by Kane (1997). Nevertheless, these validity conditions are likely to be too restrictive and are not meant to be taken as hard cutoffs (Kane (1997), Stutz (2014)).

An example of the improvement in accuracy of the RIA over the KN formula can be seen in Fig. 1, where the three theoretical DCSs are compared to experiments carried out at 59.54 keV for intermediate-Z elements (Nayak et al. (2001), Simşek (2000), Simşek et al. (2002), Yalçin (2002)). The agreement between WH and the RIA is very close. However, as will be discussed below, WH performs poorly for DCSs differential in outgoing photon energy, which are relevant for quantifying energy transfer and deposition.

For Compton scattering, Ribberfors' derivation of the RIA starts from the same lowest-order Feynman diagram as the one which yielded KN, except that the electron momentum is not taken to be zero or a constant vector. Instead, the momentum distribution of the active electron is inserted into the DCS, and an integral is performed over the angular components of the momentum distribution while assuming the latter is isotropic (Ribberfors (1975)). The presence of a momentum distribution introduces Doppler broadening, such that for a given scattering angle the outgoing photon energy spectrum is no longer a delta function at the energy given by Eq. (2), but rather is a peak that has a finite width centered at that value. Consequently, the theory predicts a cross section doubly differential in both the scattered photon angle and energy, which are treated as independent variables.

Initially the RIA expression for the DDCS of the i-th atomic (sub)shell or molecular orbital was derived to be (Ribberfors (1975))

$$\frac{\mathrm{d}^2\sigma_i}{\mathrm{d}E'\,\mathrm{d}\Omega} = N_i\,\pi r_\mathrm{e}^2\,\frac{E'}{E}\,\frac{(m_\mathrm{e}c)^2}{q}\int_{p_\mathrm{min}}^{\infty}\frac{p\,\varrho_i(p)\,\bar{X}_\mathrm{int}(p)}{E(p)}\,\mathrm{d}p, \tag{7}$$

where N_i is the number of electrons in the atomic or molecular orbital, $\varrho_i(p)$ is the radial electron density in momentum space, and $E(p)$ is the usual relativistic energy of an electron with momentum p

$$E(p) = \left[(m_\mathrm{e}c^2)^2 + (pc)^2\right]^{1/2}. \tag{8}$$

The expression for the cross-section factor $\bar{X}_\mathrm{int}(p)$ is fairly involved (Ribberfors (1975)) and shall not be reproduced here. Ribberfors suggested as a simple but acceptable approximation to use $p_\mathrm{min} = p_z$, where p_z is the projection of the electron's initial momentum $\mathbf{p}$ on the

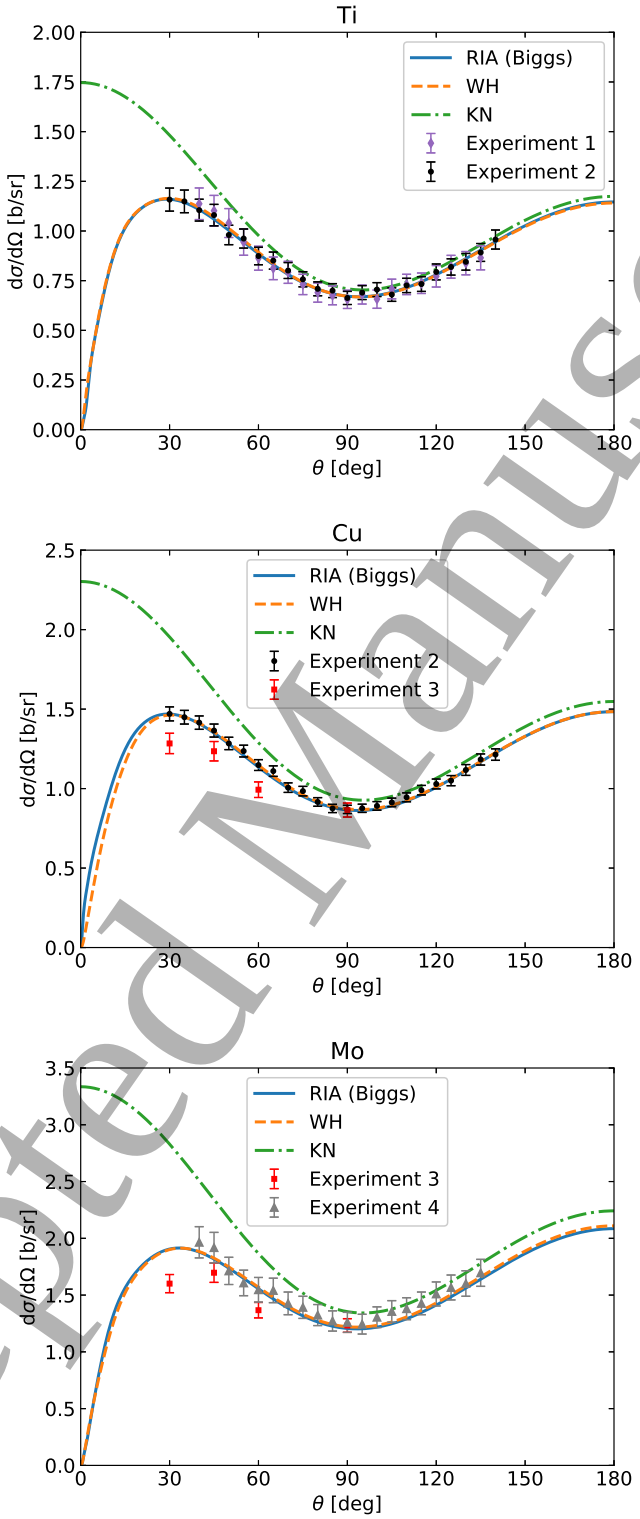

Figure 1: Whole-atom DCSs of $_{22}$Ti, $_{29}$Cu, and $_{42}$Mo. The predictions of the KN, WH, and RIA formalisms are compared to four sets of experimental data:
(1) Simşek et al. (2002) (purple diamonds); (2) Yalçin (2002) (black circles); (3) Nayak et al. (2001) (red squares); (4) Simşek (2000) (grey triangles). The measurements were done using the 59.54 keV γ-rays emitted during the decay of ^{241}Am.

direction of the scattering vector $-\mathbf{q}$, i.e.

$$p_z = -\frac{\mathbf{p}\cdot\mathbf{q}}{q} = \frac{EE'(1-\cos\theta) - m_\mathrm{e}c^2(E-E')}{c^2 q}. \tag{9}$$

An exact analytical expression for $p_{\min}$ was later explicitly given by Bell (1989), but we have employed Ribberfors' approximation because the resulting differences in the DDCSs were negligible.

In calculations of integrated cross sections (ICS) where the DDCS is integrated over E' and Ω, the additional momentum integral in Eq. (7) increases enormously the computing times. A simplification was further proposed by Ribberfors which enables the integration over p to be performed independently of the DDCS calculation. Eq. (7) was integrated by parts, and by far the largest term was found to be proportional to $J_i(p_z)\,\bar{X}_{\mathrm{int}}(p_z)/E(p_z)$, where $J_i(p_z)$ is the CP (see following subsection). The simplification consists in dropping the small remaining terms in the integration by parts, which enables to factor out the initial electron momentum dependence from the kinematics of the scattering process. Then

$$\frac{\mathrm{d}^2\sigma_i}{\mathrm{d}E'\,\mathrm{d}\Omega} = N_i\,\frac{r_\mathrm{e}^2}{2}\,\frac{E'}{E}\,\frac{(m_\mathrm{e}c)^2}{q}\,\frac{\bar{X}(R,R')}{E(p_z)}\,J_i(p_z)\,\Theta(E-E'-U_i), \tag{10}$$

where U_i is the binding energy of the i-th atomic or molecular orbital, and the Heaviside step function $\Theta(E-E'-U_i)$ ensures that the DDCS drops to zero when the energy transfer $E-E'$ is less than U_i. The now simplified cross-section factor $\bar{X}(R,R')$ is given by

$$\bar{X}(R,R') = \frac{R}{R'} + \frac{R'}{R} + 2\left(\frac{1}{R} - \frac{1}{R'}\right) + \left(\frac{1}{R} - \frac{1}{R'}\right)^2, \tag{11}$$

where

$$R = \frac{E}{m_\mathrm{e}c^2}\left\{\left[1 + \left(\frac{p_z}{m_\mathrm{e}c}\right)^2\right]^{1/2} + \frac{E - E'\cos\theta}{cq}\,\frac{p_z}{m_\mathrm{e}c}\right\} \tag{12}$$

and

$$R' = R - \frac{EE'}{(m_\mathrm{e}c^2)^2}\,(1-\cos\theta). \tag{13}$$

We have calculated DDCSs using the full (Eq. (7)) and simplified (Eq. (10)) forms of the RIA for various θ and E which cover the entire range of interest. Unexpectedly, we found that the full RIA seems to display the so-called infrared divergences, whereby for small θ the DDCS diverges as $E' \to 0$. This effect is much more pronounced when the primary photon energy E is low.

Although their effects have not yet been experimentally confirmed for the Compton interaction (see the review article (Bergstrom Jr & Pratt (1997))), infrared divergences are well understood within QED and are predicted whenever there is a pair of processes which would be the same except for one of them having an additional photon in the final state (Jauch & Rohrlich (1976)). In the limit of low outgoing photon energy, a detector (which necessarily has a finite energy resolution) cannot distinguish between the two processes,

due to the potential presence of undetected low-energy photons. It is therefore artificial and unphysical to treat these indistinguishable events as different types of interactions, and doing so leads to divergences at low scattered photon energies (Jauch & Rohrlich (1976)). In the S-matrix approach where the Compton interaction occurs in the field of an atom, the associated process which has one fewer photon in the final state is the photoelectric effect. It turns out that the lowest-order diagram for the Compton interaction is directly related to the first-order radiative corrections to atomic photoeffect, and the infrared divergences from these two terms have been shown to (partially) cancel (McEnnan & Gavrila (1977), Botto & Gavrila (1982)) so that their sum is finite.

However, while the above is relevant for Compton scattering with bound electrons, the RIA is based upon the assumption of free electrons (which nevertheless have the momentum distribution of bound electrons). For Compton scattering involving free electrons there is no corresponding process with one fewer photon in the final state. One might then expect the RIA to not exhibit infrared divergences, and in fact it has been stated previously that the RIA should in principle not be able to account for such divergences (Bergstrom Jr & Pratt (1997), Florescu & Gavrila (2000), Pratt et al. (2010)).

We have integrated the full and simplified RIA DDCSs in the Compton peak range near $E' = E_{\mathrm{C}}$ (which contains no divergences), and found differences of 0.3% or less in the DCSs, which are smaller than the differences resulting from using atomic vs. molecular Compton profiles (as can be seen in Figs. 3 and 4 below). We have thus opted to compute all results within this paper using the simplified RIA, Eq. (10), also because it is not possible to directly integrate the full RIA over the entire scattered energy and angle ranges for ICS calculations. Besides, the simplified expression for the RIA DDCS is the one that has been exclusively used in calculations of Compton cross sections in the literature (Stutz (2014), Rao et al. (2004), The International Commission on Radiation Units and Measurements (2016), Rao et al. (2002, 2003)). The divergences observed in the full RIA call for further investigation, but such an undertaking is beyond the scope of the present work.

2.4. Compton profiles

The (isotropic) CP is an integral of the spherically-averaged electron momentum density $\varrho_i(p)$ of the considered atomic or molecular orbital,

$$J_i(p_z) = 2\pi \int_{|p_z|}^{\infty} \varrho_i(p)\, p \, \mathrm{d}p. \tag{14}$$

By definition, the CP is symmetric and the following normalization condition is satisfied,

$$\int_{-\infty}^{+\infty} J_i(p_z)\, \mathrm{d}p_z = 1. \tag{15}$$

Simple analytical forms for the CPs have been proposed in the past, e.g. by Ribberfors & Berggren (1982), where the integration over CPs is approximated by an elementary linear function. Brusa et al. (1996) also introduced analytical functions for the CPs in order to

simplify the random sampling in Monte Carlo codes. A comparison of RIA results with and without CP simplifications has found that deviations can be significant, especially at low incident photon energies and large scattering angles (Stutz (2014)).

When such approximations are not necessary, data for CPs of atomic (sub)shells are typically taken from the comprehensive tabulation by Biggs et al. (1975), which were calculated using non-relativistic ($1 \leqslant Z \leqslant 36$) and relativistic ($36 \leqslant Z \leqslant 102$) Hartree–Fock wavefunctions. However, the sparse tabulation and small number of significant figures in the data means that errors of up to 1% can occur in the interpolation procedure alone (although for most subshells the error is closer to 0.1%). Therefore, in this work we do not use the Biggs *et al.* tabulation of CPs for atomic (sub)shells, but instead we calculate CPs for both atomic and molecular orbitals within the Hartree–Fock framework outlined below.

Adopting the unrestricted Hartree–Fock description, the wave function of an atomic or molecular system with N electrons is expressed as a Slater determinant constructed with a set $\{\Phi_i\}_{i=1,\ldots,N}$ of one-electron atomic or molecular spin-orbitals. The Fourier transforms of the corresponding space orbitals are

$$\widetilde{\Phi}_i(\mathbf{p}) = \frac{1}{(2\pi\hbar)^{3/2}} \int \mathrm{d}^3\mathbf{r}\, \mathrm{e}^{-\mathrm{i}\mathbf{p}\cdot\mathbf{r}/\hbar}\, \Phi_i(\mathbf{r}), \tag{16}$$

so that the spherically-averaged momentum distribution can be written as

$$\varrho_i(p) = p^2 \int_{4\pi} \mathrm{d}\hat{\mathbf{p}} \left|\widetilde{\Phi}_i(\mathbf{p})\right|^2. \tag{17}$$

Under the linear combination of atomic orbitals approximation, the space orbitals are expanded in a non-complete basis set $\{\varphi_s\}_{s=1,\ldots,M}$. Then $\varrho_i(p)$ can be computed as a sum of contributions from the basis functions. Here we have chosen the Cartesian Gaussian-type orbitals (García de la Vega et al. (1997)), whose Fourier transform was derived by Kaijser & Smith Jr (1977). The size of the adopted basis set was cc-pVTZ (Dunning Jr (1989), Woon & Dunning Jr (1993)). The contributions to $\varrho_i(p)$ are given by integrals that can be found in (García de la Vega et al. (1997)). For the ground state of molecules the optimized equilibrium distance was selected. The calculations have been carried out employing the GAUSSIAN03 program (Frisch et al. (2004)).

The momentum distributions ensuing from these self-consistent calculations are tabulated on a very dense grid of p values, with at least 100 times more points than the tabulation of Biggs et al. (1975) and with 9 significant figures. Since the spin of the electrons was taken into account, the CP was slightly different for spin up and spin down electrons in the same atomic or molecular space orbital. In our cross section calculations, we simply added the contribution from all electrons (spin up and down) within a given space orbital.

In the case of graphite, we differentiate the latter from atomic carbon by considering, as was done in ICRU Report 90 (The International Commission on Radiation Units and Measurements (2016)), that one of the 2p electrons is a conduction electron. We further assume that these conduction electrons form a degenerate free-electron gas (feg), whose CP

is given by (Cooper (1985))

$$J^{\mathrm{feg}}(p_z) = \frac{3}{4p_{\mathrm{F}}}\left(1 - \frac{p_z^2}{p_{\mathrm{F}}^2}\right)\Theta(p_{\mathrm{F}} - |p_z|), \tag{18}$$

where $p_{\mathrm{F}} \equiv \hbar(3\pi^2\rho_{\mathrm{e}})^{1/3}$ is the Fermi momentum, and ρ_{e} is the number of electrons per unit volume, which is proportional to the mass density of the material (for graphite we took the grain density of 2.265 g/cm^3 (The International Commission on Radiation Units and Measurements (2016))). The remaining five electrons in graphite are treated as being identical to the corresponding electrons in the carbon atom.

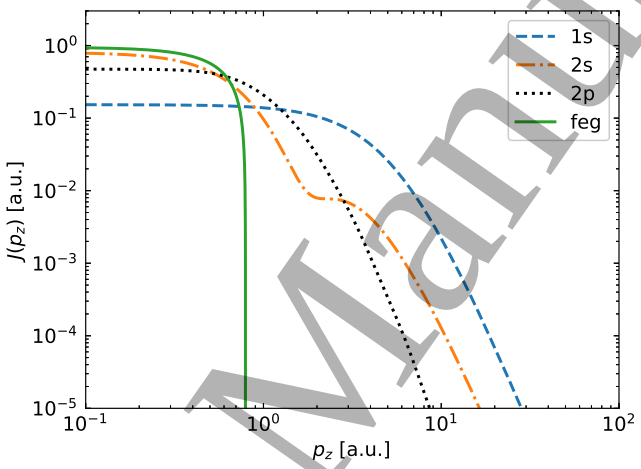

Figure 2: CPs for the three occupied (sub)shells of the carbon atom, calculated from unrestricted Hartree–Fock wavefunctions, and for the conduction electron (feg) . All quantities are in atomic units.

In Fig. 2 we show the unrestricted Hartree–Fock CPs for the occupied (sub)shells of graphite, including the conduction band. We see that more tightly bound shells have a broader momentum distribution, as would be expected since the electrons in these shells move faster, and also because the probability distribution in position space (which is the inverse Fourier transform of the momentum distribution) is more sharply peaked for inner shells.

2.5. Dosimetric quantities

In this subsection we review the fundamental dosimetric quantities of interest, following standard definitions and conventions (Seltzer (1993), Abdel-Rahman & Podgorsak (2010)). The mass attenuation coefficient is defined as

$$\frac{\mu}{\rho} = \frac{N_{\mathrm{A}}}{\mathcal{M}}\sum_j \sigma_j, \tag{19}$$

where ρ is the mass density of the medium, $N_{\rm A}$ is the Avogadro constant, $\mathcal{M}$ is the molar mass of the atoms or molecules that make up the medium, and σ_j is the ICS for the interaction of type j. The mass energy-transfer coefficient is

$$\frac{\mu_{\rm tr}}{\rho} = \sum_j f_j \frac{\mu_j}{\rho}, \tag{20}$$

where f_j is the average fraction of the photon energy transferred to kinetic energy of the charged particles, which is defined differently for each interaction type. For the Compton interaction

$$f_{\rm C} = 1 - \frac{\langle E' \rangle + \mathcal{X}}{E}, \tag{21}$$

where $\langle E' \rangle$ is the average energy of the scattered photons

$$\langle E' \rangle = \frac{1}{\sigma_{\rm C}} \int_{E_{\rm min}}^{E_{\rm max}} E' \frac{{\rm d}\sigma_{\rm C}}{{\rm d}E'} \, {\rm d}E', \tag{22}$$

with $E_{\rm min}$ and $E_{\rm max}$ being different for different theories depending on the allowed range of scattered photon energies, and $\mathcal{X}$ is the average energy of the fluorescence radiation emitted per absorbed photon. In principle, the calculation of $\mathcal{X}$ involves following the entire cascade of x-rays emitted in radiative transitions resulting from the initial vacancy. However, since here we are only dealing with biologically relevant materials which are made of low-Z elements, $\mathcal{X} \ll \langle E' \rangle < E$ and only the x-ray energy emitted directly from the filling of the initial vacancy needs to be considered. We therefore approximate $\mathcal{X}$ as (Seltzer (1993))

$$\mathcal{X}(E) = \sum_n p_n(E) \, \mathcal{X}_n^{\rm cascade} \approx \sum_n p_n(E) \, \mathcal{X}_n^{\rm direct}, \tag{23}$$

where (sub)shell n is where the initial vacancy was created, $p_n(E) = \sigma_n(E)/\sigma(E)$ is the probability of Compton interaction for this (sub)shell, and

$$\mathcal{X}_n^{\rm direct} = \omega_n \sum_m \frac{\Gamma_{nm}}{\Gamma_{n,{\rm total}}} E_{nm}, \tag{24}$$

where ω_n is the fluorescence yield, the sum extends over the higher shells involved in the radiative transitions, Γ_{nm} is the emission rate for radiative transitions between (sub)shells n and m, and the x-ray energy E_{nm} is to a good approximation equal to the difference in binding energies of the two (sub)shells. Furthermore, due to the low fluorescence yields and emission rates of the L subshells, we ultimately only included the contribution from an initial K-shell vacancy. The fluorescence yields and emission rates were taken from the tables of Krause (1979) and Scofield (1974), respectively.

Given the energy interval of present concern (1 keV–1 MeV), the other relevant interaction mechanism is the photoelectric effect (pe), for which the energy-transfer fraction is

$$f_{\rm pe} = 1 - \frac{\mathcal{X}}{E}. \tag{25}$$

The pe ICSs were taken from the PENELOPE database (Salvat (2019)), which was calculated resorting to standard first-order perturbation theory but with the normalization screening correction included (Sabbatucci & Salvat (2016)).

Finally, we calculate the effect on the total mass energy-absorption coefficient $\mu_{\rm en}/\rho$, defined as

$$\frac{\mu_{\rm en}}{\rho} = (1-g)\,\frac{\mu_{\rm tr}}{\rho}, \tag{26}$$

where g is the average fraction of the kinetic energy of secondary charged particles which is subsequently lost to radiative processes. Instead of defining a g_i for each type of interaction, as done in (Seltzer (1993)), we employed the user code `g` of the `EGSnrc` system (Rogers et al. (2003)) to compute a value for g for a given material at each photon energy E. For low-Z materials, g has a very small effect on $\mu_{\rm en}/\rho$, being typically around 0.2% or 0.3% at $E =$ 1 MeV, and an order of magnitude smaller for energies of a few hundred keV and below (Andreo et al. (2017)).

3. Results

3.1. Differential cross sections

The RIA DDCS, Eq. (10), was computed with a simple Python script, while the CP was interpolated using the interpolation package from SciPy (Virtanen et al. (2020)). Integration of the DDCS and DCS were performed with the `simps` function of the SciPy integration package (Virtanen et al. (2020)), which implements Simpson's rule. Given the dense interpolation and integration grids we used, and that we are dealing with slowly-varying functions, errors from the above numerical procedures are entirely negligible.

In computing the RIA cross sections using atomic CPs for graphite and the molecules of air, we simply simply added up the contribution of each atomic subshell. However, for water we followed the procedure for the "molecular IA" calculation described in the ICRU Report 90, whereby we constructed molecular orbitals from linear combinations of atomic orbitals, with coefficients taken from (Siegbahn (1969)). This provides a more stringent evaluation of the effect of using molecular CPs as opposed to linear combinations of atomic CPs. The atomic binding energies we used are those recommended by Carlson (1975), and the molecular orbital binding energies are the experimental values tabulated by Rudd et al. (1992). For the molecular composition of air, we used the fractions by weight found in the NIST database (Berger et al. (1998)).

In Fig. 3, we plot the DCS differential in scattering angle for graphite and water at 2, 10, and 50 keV. As expected, we observe that the DCS becomes more forward peaked at higher energies as backscattering is suppressed. Another well-known feature is that accounting for binding effects forces the DCS to go to zero at $\theta = 0$. Indeed, since we model graphite as having one conduction electron which is free, its atomic DCS does not go to zero at $\theta = 0$, same as for the KN DCS. One could expect the conduction electron's DCS at $\theta = 0$ to go to

the same value as predicted by the Thomson DCS for elastic scattering of photons by free electrons. However, an unintended consequence of the RIA is that the DCS at $\theta = 0$ actually goes to one half of the Thomson DCS, due to the CP (and hence, the DDCS) being peaked at the maximum value of $E' = E$, and thus the integral over E' only covering half of the symmetric Compton peak. At low incident photon energies of about 1 keV, the KN DCS is an order of magnitude larger than the other DCSs, but this gap diminishes as the energy increases. The WH DCS is in excellent agreement with the atomic RIA DCS, which is in turn is very close to the molecular RIA except when a conduction electron is present. The DCS for air displays the same behaviour as described above, and the plots are qualitatively very similar to water and atomic carbon (results not shown).

If we now look at the DCS differential in scattered photon energy for graphite in Fig. 4, we first note that both KN and WH predict a minimum E' corresponding to 180° backscattering, whereas the RIA does not. We also note that since the RIA accounts for the binding energy, there is a maximum $E'_{\max} = E - U_i$ for each (sub)shell, leading to the discontinuities clearly visible in the upper two subfigures.

At low energies, the KN DCS is many times larger than the other DCSs. Therefore, we decided not to show the KN DCS in the first panel at 1 keV, since the other DCSs would be scaled down along the y-axis and their detailed features would not be as visible. Despite the vast differences in shape between the WH and the RIA, due to the incoherent scattering function suppressing the DCS when E' approaches E, the two theories have similar ICSs. However, as we shall see below, the integrated energy-transfer CSs are quite different.

3.2. Photon interaction coefficients

Same as for the DCS in Fig. 3, we see from Figs. 5 and 6 that the choice of CPs (molecular vs atomic) has a minimal impact on μ^{C}/ρ and $\mu^{\mathrm{C}}_{\mathrm{tr}}/\rho$. Once again, the only exception is graphite, whose μ^{C}/ρ is almost three times higher than the atomic RIA at 1 keV owing to the presence of the conduction electron. When comparing our RIA results with the ICRU 90 tables for μ^{C}/ρ, we find that our calculations differ by at most a few percent from the XCOM and the S-matrix (mislabeled as '*ab initio* RIA') values for all three materials, and tend to fall somewhere between the two data sets. The only exception is at 1 keV, where differences can be closer to 10%, but above 10 keV the values are within 1% of each other. For water, our molecular RIA results are closest to the 'Molecular IA' column of Rao *et al.*, where discrepancies are within 2%, even in the low keV range. For graphite with one conduction electron, our values differ by about 1% or less from the PENELOPE tabulation. However, although we have carried out fully atomic calculations (direct sum of atomic orbital contributions) of μ^{C}/ρ, we were not able to reproduce the Rao *et al.* values for atomic carbon and 'Atomic IA' of water. In fact, our fully atomic calculations are at most 5% larger than our molecular results, while Rao *et al.*'s atomic values are higher by up to a factor of two in the low keV range. Furthermore, we could not identify a literature source supporting Rao *et al.*'s atomic IA data below 5 keV for graphite and water.

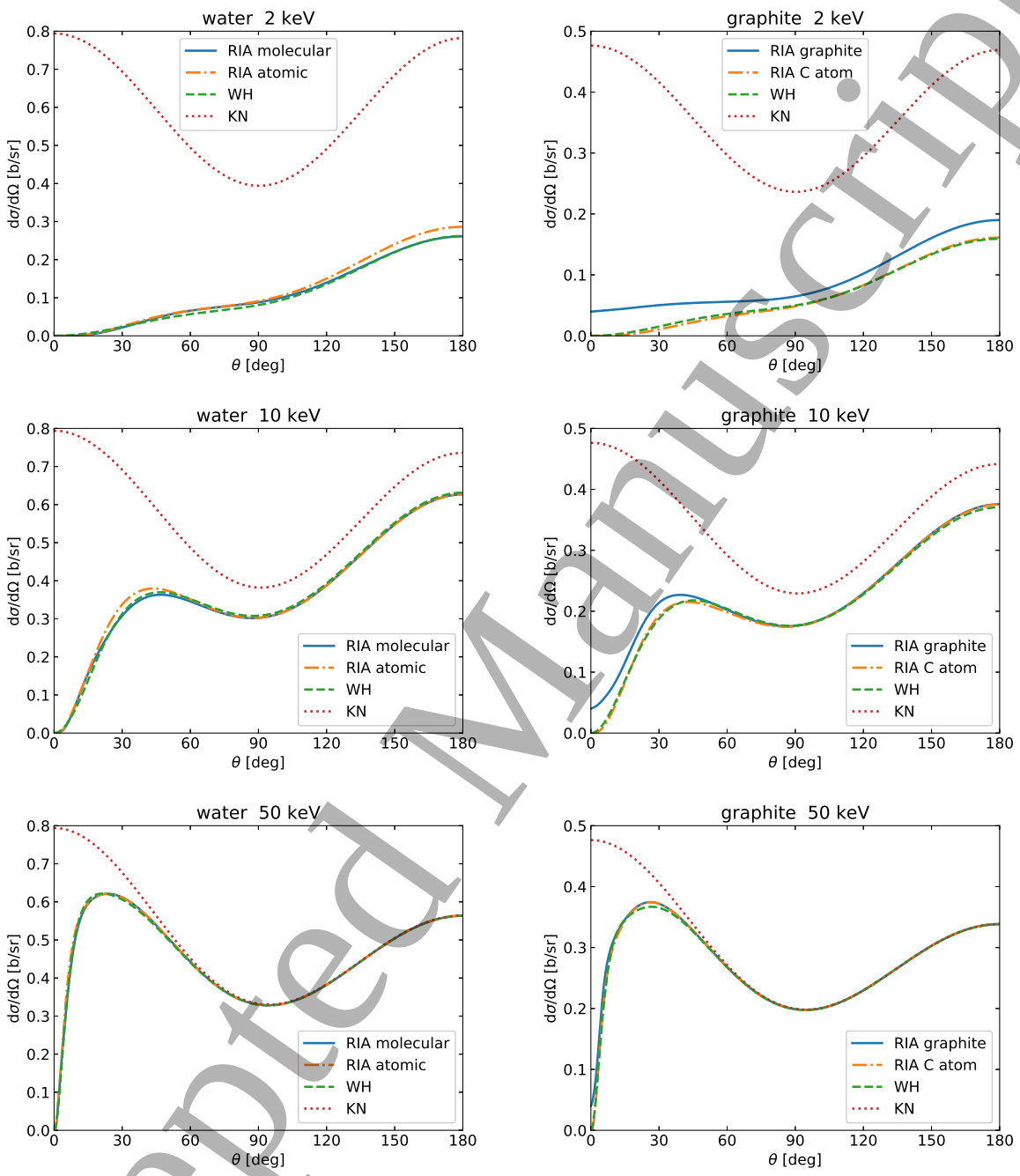

Figure 3: KN, WH, and RIA DCSs for water and graphite at three incident photon energies (2, 10, and 50 keV). For water, we compare RIA DCSs calculated using both atomic and molecular CPs from unrestricted Hartree–Fock wavefunctions. In the case of graphite we compare the RIA DCSs assuming 1 conduction electron with the RIA DCSs pertaining to atomic carbon.

On the other hand, the choice of theoretical formalism does have an impact on the Compton interaction coefficients. When looking at μ^{C}/ρ, WH binding corrections seem to

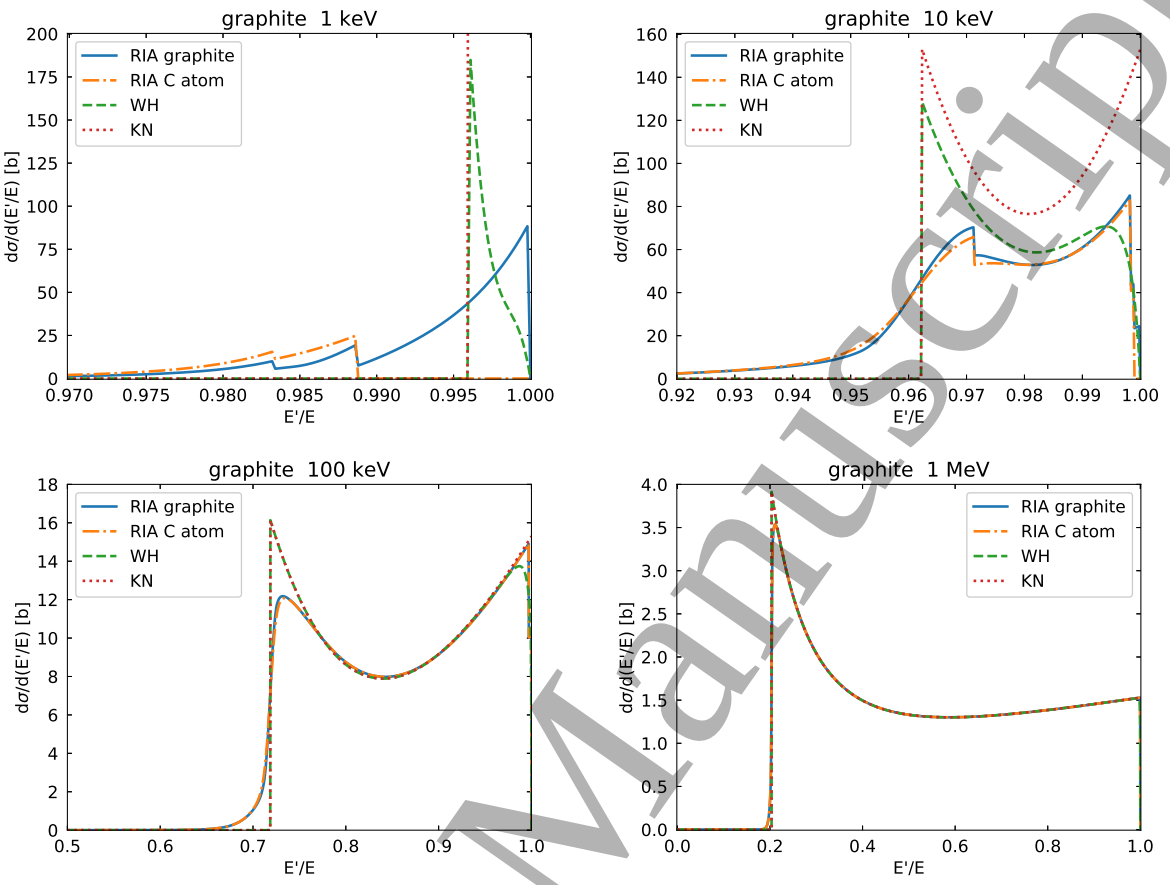

Figure 4: KN, WH, and RIA DCSs differential in scattered photon energy for graphite at four incident photon energies. The RIA DCSs were calculated for graphite with 1 conduction electron as well as for atomic carbon. Note that E' is normalized by E for a clearer presentation of the figures.

be in excellent agreement with the RIA, unlike the KN approach which is off by up to an order of magnitude. However, when considering $\mu_{\rm tr}^{\rm C}/\rho$, the WH theory actually agrees less with the RIA than the KN approximation does. This can be better understood by returning to Fig. 4, where we see that even though the areas under the WH and RIA curves are the same, the WH energy-transfer cross section would clearly be much smaller for low incident energies. The WH $\mu_{\rm tr}^{\rm C}/\rho$ can differ by a large amount from the predictions of the other models in the tens of keV range (e.g. 6–10% at 20 keV), when Compton scattering becomes the dominant interaction mechanism. Our calculated WH $\mu_{\rm tr}^{\rm C}/\rho$ values reproduce with high accuracy the data from Seltzer (1993), and our RIA calculations are also in good agreement with previously published results (Stutz (2014), Brusa et al. (1996)). To our knowledge, the appreciable differences between the WH and RIA predictions for energy transfer were noticed by Ribberfors & Alm Carlsson (1985) but have not been widely reported in the literature.

Ultimately, with decreasing photon energy the energy transfer resulting from the

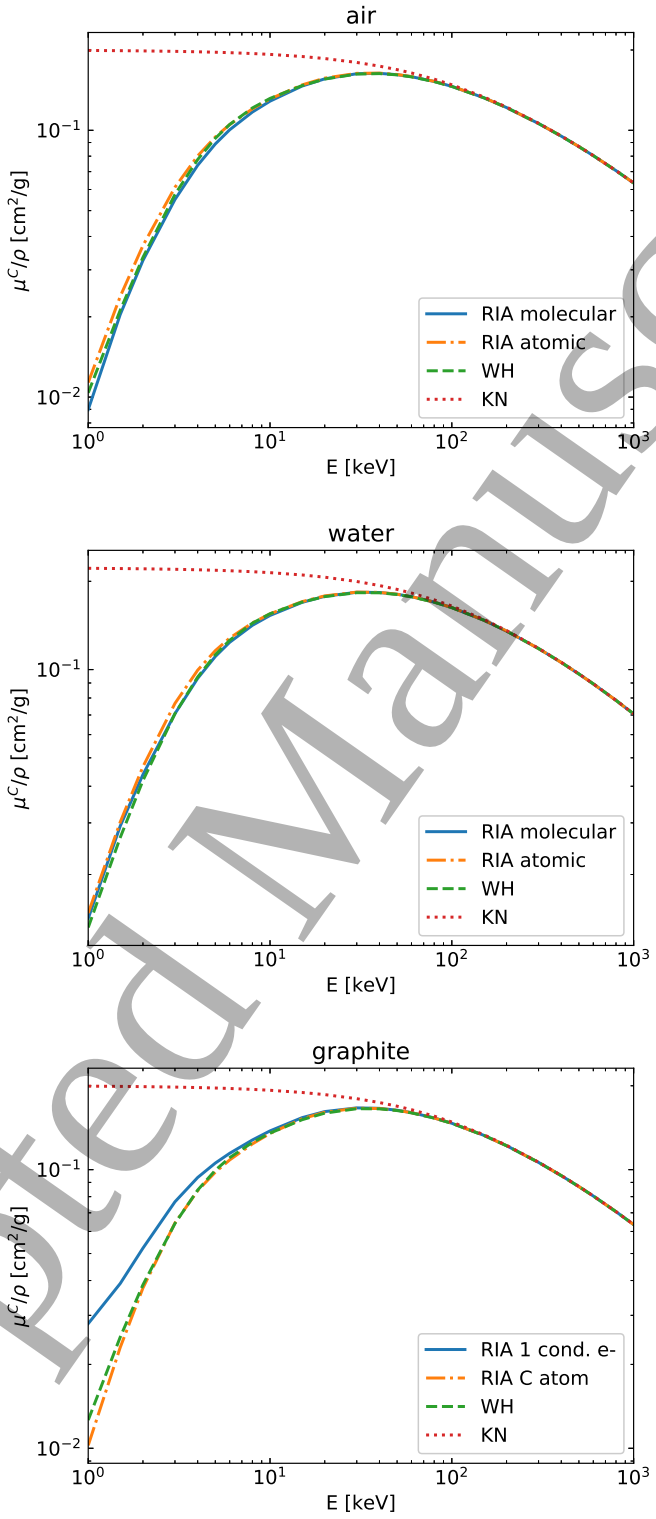

Figure 5: Partial mass attenuation coefficient μ^{C}/ρ for air, water, and graphite.

photoelectric effect (pe) will overwhelm the diminishing energy transfer from the Compton interaction in the low tens of keV range, hence the differences in the total μ_{en}/ρ resulting from the choice of theoretical Compton model are no larger than 0.4%, and the differences between WH and the other two formalisms are no longer prominent. In Fig. 7 we have only considered the μ_{en}/ρ which uses the molecular RIA since the one with the atomic RIA would be indistinguishable when plotted in the figure. Therefore, the uncertainty in μ_{en}/ρ introduced by using different Compton models is significantly smaller than the uncertainty from the pe (Andreo et al. (2012)).

4. Conclusions

In summary, we calculated differential and integrated cross sections for the Compton interaction within the KN, WH, and RIA formalisms, for three materials of dosimetric interest in the 1 keV to 1 MeV interval. We compared using molecular versus atomic CPs in the RIA, but found no significant differences in the DCS. However, assuming one conduction electron in graphite does result in significant deviations at low energies from calculations for the carbon atom, since we are essentially treating one of the electrons as free, with a momentum distribution corresponding to that of a degenerate free-electron gas.

We then calculated mass energy-transfer coefficients, and surprisingly found the WH theory to differ from the other models by up to an order of magnitude at low energies. This is due to the large differences in the shape of the WH and RIA DCSs differential in outgoing photon energy, despite their integrated cross sections being very close. We therefore conclude that while the approach of multiplying the KN DCS by the incoherent scattering function seems accurate for calculating the DCS and the ICS, it does not seem appropriate for calculating the energy-transfer cross section. Fortunately, when considering the total (Compton + pe) μ_{en}/ρ, the pe contribution dominates in the energy interval where the WH prediction fails, so that the overall differences in μ_{en}/ρ from using different Compton models are within 0.4%.

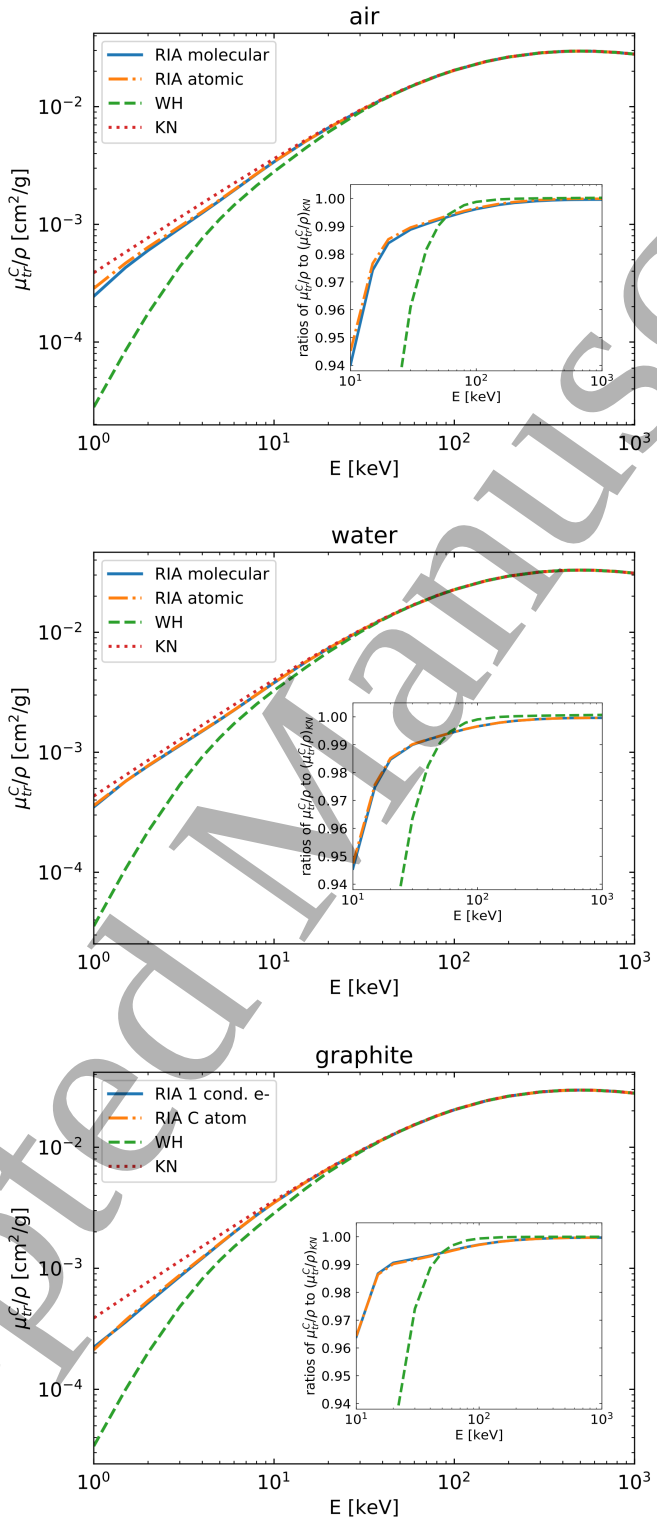

Figure 6: Partial mass energy-transfer coefficient $\mu_{\mathrm{tr}}^{\mathrm{C}}/\rho$ for air, water, and graphite, calculated within the KN, WH, and RIA (with molecular and atomic CP) models. The insets show, above 10 keV, the WH and RIA curves normalized by the KN data, with a linear y-axis to better visualize the percent differences between the models.

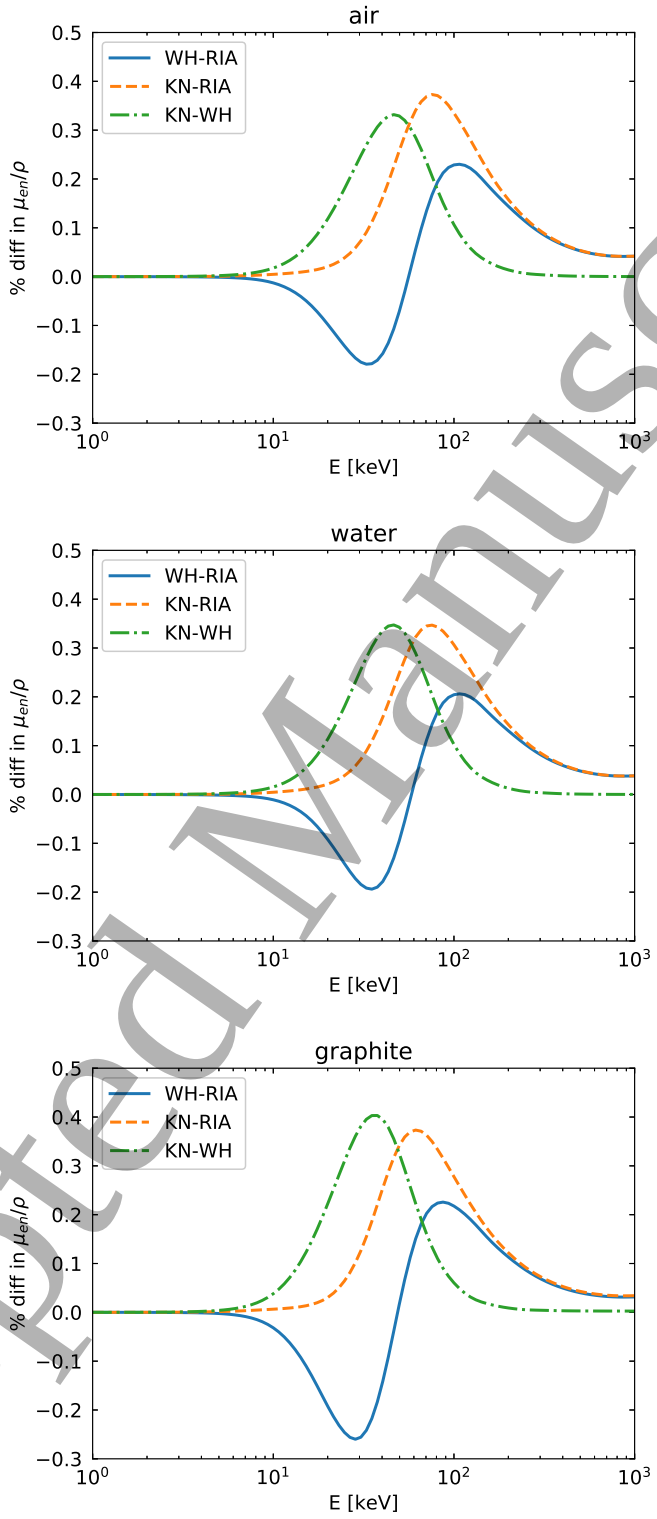

Figure 7: Percent difference in mass energy-absorption coefficients, μ_{en}/ρ, including the photoelectric effect, between pairs of Compton models.

Acknowledgements

We have benefited from enlightening discussions with Dr. Paul Bergstrom Jr (National Institute of Standards and Technology). XJW acknowledges support from the Natural Sciences and Engineering Research Council (NSERC) PGS D award. This work was partially funded by the CREATE Medical Physics Research Training Network grant of the NSERC (Grant number: 432290) and by NSERC operating grant RGPIN-2019-06746. JMF-V thanks the support by the Spanish Ministerio de Ciencia, Innovación y Universidades, Grant No. PGC2018-096788-B-I00.

References

Abdel-Rahman, W. & Podgorsak, E. B. (2010), 'Energy transfer and energy absorption in photon interactions with matter revisited: A step-by-step illustrated approach', *Radiat. Phys. Chem.* **79**, 552–566.

Alm Carlsson, G., Berggren, K. F., Carlsson, C. A., Matscheko, G. & Ribberfors, R. (1989), 'The Compton spectrometer', *Int. J. Quantum Chem.* **XXXV**, 721–734.

Andreo, P. (2019), 'Data for the dosimetry of low- and medium-energy kV x rays', *Phys. Med. Biol.* **64**(20), 205019.

Andreo, P., Burns, D. T., Nahum, A. E., Seuntjens, J. & Attix, F. H. (2017), *Fundamentals of Ionizing Radiation Dosimetry*, 2nd edn, Wiley-Vch.

Andreo, P., Burns, D. T. & Salvat, F. (2012), 'On the uncertainties of photon mass energy-absorption coefficients and their ratios for radiation dosimetry', *Phys. Med. Biol.* **57**, 2117–2136.

Bell, F. (1989), 'Double and triple differential cross sections for K-shell ionisation by relativistic electron impact', *J. Phys. B: At. Mol. Opt. Phys.* **22**, 287–297.

Benmakhlouf, H., Bouchard, H., Fransson, A. & Andreo, P. (2011), 'Backscatter factors and mass energy-absorption coefficient ratios for diagnostic radiology dosimetry', *Phys. Med. Biol.* **56**, 7179–7204.

Berger, M. J., Coursey, J. S., Zucker, M. A. & Chang, J. (1998), *Stopping-power and range tables for electrons, protons, and helium ions*, NIST Physics Laboratory Gaithersburg, MD.

Berger, M. J. & Hubbell, J. H. (1987), *XCOM: photon cross sections on a personal computer, Report NBSIR 87–3597*, National Bureau of Standards, Gaithersburg, MD.

Bergstrom Jr, P. M. & Pratt, R. H. (1997), 'An overview of the theories used in Compton scattering calculations', *Radiat. Phys. Chem.* **50**(1), 3–29.

Bergstrom Jr, P. M., Suric, T., Pisk, K. & Pratt, R. H. (1993), 'Compton scattering of photons from bound electrons: full relativistic independent-particle-approximation calculations', *Phys. Rev. A* **48**(2), 1134–1162.

Biggs, F., Mendelsohn, L. B. & Mann, J. B. (1975), 'Hartree-Fock Compton profiles for the elements', *At. Data Nucl. Data Tables* **16**, 201–309.

Botto, D. J. & Gavrila, M. (1982), 'Radiative corrections to atomic photoeffect and tip bremsstrahlung. III', *Phys. Rev. A* **26**(1), 237–249.

Brusa, D., Stutz, G., Riveros, J. A., Fernández-Varea, J. M. & Salvat, F. (1996), 'Fast sampling algorithm for the simulation of photon Compton scattering', *Nucl. Instrum. Methods A* **379**, 167–175.

Büermann, L. & Burns, D. T. (2009), 'Air-kerma cavity standards', *Metrologia* **46**, S24–S38.

Burns, D. T. & Büermann, L. (2009), 'Free-air ionization chambers', *Metrologia* **46**, S9–S23.

Carlson, T. A. (1975), *Photoelectron and Auger Spectroscopy*, Springer, New York.

Cooper, M. J. (1985), 'Compton scattering and electron momentum determination', *Rep. Prog. Phys.* **48**(4), 415–481.

Cullen, D. E., Chen, M. H., Hubbell, J. H., Perkins, S. T., Plechaty, E. F., Rathkopf, J. A. & Scofield, J. H. (1989), Tables and graphs of photon-interaction cross sections from 10 eV to 100 GeV derived from the LLNL Evaluated Photon Data Library (EPDL), Technical Report OSTI-6901928, Lawrence Livermore National Laboratory.

Cullen, D. E., Hubbell, J. H. & Kissel, L. (1997), EPDL97: the evaluated photo data library '97 version, Technical Report OSTI-295438, Lawrence Livermore National Laboratory.

Dunning Jr, T. H. (1989), 'Gaussian basis sets for use in correlated molecular calculations. I. The atoms boron through neon and hydrogen', *J. Chem. Phys.* **90**, 1007–1023.

Florescu, V. & Gavrila, M. (2000), 'Soft-photon emission in extreme-relativistic Compton scattering by K-shell electrons and connection to photoeffect', *Radiat. Phys. Chem.* **59**, 127–136.

Frisch, M. J., Trucks, G. W., Schlegel, H. B., Scuseria, G. E., Robb, M. A., Cheeseman, J. R., Montgomery, Jr., J. A., Vreven, T., Kudin, K. N., Burant, J. C., Millam, J. M., Iyengar, S. S., Tomasi, J., Barone, V., Mennucci, B., Cossi, M., Scalmani, G., Rega, N., Petersson, G. A., Nakatsuji, H., Hada, M., Ehara, M., Toyota, K., Fukuda, R., Hasegawa, J., Ishida, M., Nakajima, T., Honda, Y., Kitao, O., Nakai, H., Klene, M., Li, X., Knox, J. E., Hratchian, H. P., Cross, J. B., Bakken, V., Adamo, C., Jaramillo, J., Gomperts, R., Stratmann, R. E., Yazyev, O., Austin, A. J., Cammi, R., Pomelli, C., Ochterski, J. W., Ayala, P. Y., Morokuma, K., Voth, G. A., Salvador, P., Dannenberg, J. J., Zakrzewski, V. G., Dapprich, S., Daniels, A. D., Strain, M. C., Farkas, O., Malick, D. K., Rabuck, A. D., Raghavachari, K., Foresman, J. B., Ortiz, J. V., Cui, Q., Baboul, A. G., Clifford, S., Cioslowski, J., Stefanov, B. B., Liu, G., Liashenko, A., Piskorz, P., Komaromi, I., Martin, R. L., Fox, D. J., Keith, T., Al-Laham, M. A., Peng, C. Y., Nanayakkara, A., Challacombe, M., Gill, P. M. W., Johnson, B., Chen, W., Wong, M. W., Gonzalez, C. & Pople, J. A. (2004), 'Gaussian 03, Revision D.02'. Gaussian, Inc., Wallingford, CT.

García de la Vega, J. M., Miguel, B. & Ramírez, G. (1997), 'Two-center p-space integrals: diatomic molecular moments', *J. Math. Chem.* **21**, 211–222.

Hill, R., Healy, B., Holloway, L., Kuncic, Z., Thwaites, D. & Baldock, C. (2014), 'Advances in kilovoltage x-ray beam dosimetry', *Phys. Med. Biol.* **59**, R183–R231.

Hubbell, J. H. (1997), 'Summary of existing information on the incoherent scattering of photons, particularly on the validity of the use of the incoherent scattering function', *Radiat. Phys. Chem.* **50**, 113–124.

Hubbell, J. H. (2006), 'Review and history of photon cross section calculations', *Phys. Med. Biol.* **51**, 245–262.

Hubbell, J. H. & Seltzer, S. M. (1995), Tables of x-ray mass attenuation coefficients and mass energy-absorption coefficients 1 keV to 20 MeV for elements Z= 1 to 92 and 48 additional substances of dosimetric interest, Technical Report NISTIR 5632, National Bureau of Standards and Technology, Gaithersburg, MD.

Hubbell, J. H., Veigele, W. J., Briggs, E. A., Brown, R. T., Cromer, D. T. & Howerton, R. J. (1975), 'Atomic form factors, incoherent scattering functions, and photon scattering cross sections', *J. Phys. Chem. Ref. Data* **4**(3), 471–538. Corrected in Erratum Hubbell et al. (1977).

Hubbell, J. H., Veigele, W. J., Briggs, E. A., Brown, R. T., Cromer, D. T. & Howerton, R. J. (1977), 'Erratum: atomic form factors, incoherent scattering functions, and photon scattering cross sections', *J. Phys. Chem. Ref. Data* **6**(2), 615–616.

Jauch, J. M. & Rohrlich, F. (1976), *The Theory of Photons and Electrons. The Relativistic Quantum Field Theory of Charged Particles with Spin One-half*, Springer, New York.

Johns, P. C. (2002), Medical x-ray imaging with scattered photons, Vol. TD01, pp. 355–357.

Kaijser, P. & Smith Jr, V. H. (1977), 'Evaluation of momentum distributions and Compton profiles for atomic and molecular systems', *Advances in Quantum Chemistry* **10**, 37–76.

Kane, P. P. (1997), 'Experimental studies of inelastic X-ray and γ-ray scattering', *Rad. Phys. Chem.* **50**(1), 31–62.

Klein, O. & Nishina, Y. (1929), 'Über die Streuung von Strahlung durch freie Elektronen nach der neuen relativistischen Quantendynamik von Dirac', *Z. Phys.* **52**, 853–868.

Krause, M. O. (1979), 'Atomic radiative and radiationless yields for K and L shells', *J. Phys. Chem. Ref. Data* **8**(2), 307–327.

McEnnan, J. & Gavrila, M. (1977), 'Radiative corrections to the atomic photoeffect', *Phys. Rev. A* **15**(4), 15–37.

Nayak, N. G., Pinto, G. & Siddappa, K. (2001), 'Incoherent scattering of 59.54 keV γ-rays at small momentum transfers', *Radiat. Phys. Chem.* **60**, 555–564.

O'Meara, J. M., Chettle, D. R., McNeill, F. E., Prestwich, W. V. & Svensson, C. E. (1998), 'Monte Carlo simulation of source-excited *in vivo* x-ray fluorescence measurements of heavy metals', *Phys. Med. Biol.* **43**, 1413–1428.

Pratt, R. H., LaJohn, L. A., Florescu, V., Suric, T., Chatterjee, B. K. & Roy, S. C. (2010), 'Compton scattering revisited', *Radiat. Phys. Chem.* **79**, 124–131.

Rao, D. V., Seltzer, S. M. & Bergstrom Jr, P. M. (2004), 'Compton scattering cross-sections for individual subshells for a few elements of biological interest in the energy region 5 keV–10 MeV', *Radiat. Phys. Chem.* **70**, 479–489.

Rao, D. V., Takeda, T., Itai, Y., Akatsuka, T., Cesareo, R., Brunetti, A. & Gigante, G. E. (2002), 'Doppler broadening and its contribution to Compton energy-absorption cross sections: An analysis of the Compton component in terms of mass-energy absorption coefficient', *J. Phys. Chem. Ref. Data* **31**(3), 769–818. Corrected in Erratum Rao et al. (2003).

Rao, D. V., Takeda, T., Itai, Y., Akatsuka, T., Cesareo, R., Brunetti, A. & Gigante, G. E. (2003), 'Erratum: Doppler broadening and its contribution to Compton energy-absorption cross sections: An analysis of the Compton component in terms of mass-energy absorption coefficient', *J. Phys. Chem. Ref. Data* **32**(2), 917.

Ribberfors, R. (1975), 'Relationship of the relativistic Compton cross section to the momentum distribution of bound electron states', *Phys. Rev. B* **12**(6), 2067–2074. Corrected in Erratum Ribberfors (1976).

Ribberfors, R. (1976), 'Erratum: Relationship of the relativistic Compton cross section to the momentum distribution of bound electron states', *Phys. Rev. B* **13**(2), 950.

Ribberfors, R. & Alm Carlsson, G. (1985), 'Compton component of the mass-energy absorption coefficient: corrections due to the energy broadening of Compton-scattered photons', *Rad. Res.* **101**, 47–59.

Ribberfors, R. & Berggren, K. F. (1982), 'Incoherent-x-ray-scattering functions and cross sections by means of a pocket calculator', *Phys. Rev. A* **26**(6), 3325–3333.

Rogers, D. W. O., Kawrakow, I., Seuntjens, J. P., Walters, B. R. B. & Mainegra-Hing, E. (2003), 'NRC user codes for EGSnrc', *NRCC Report PIRS-702 (Rev. B)* .

Rudd, M. E., Kim, Y.-K., Madison, D. H. & Gay, T. J. (1992), 'Electron production in proton collisions with atoms and molecules: energy distributions', *Rev. Mod. Phys.* **64**(2), 441–490.

Sabbatucci, L. & Salvat, F. (2016), 'Theory and calculation of the atomic photoeffect', *Radiat. Phys. Chem.* **121**, 122–140.

Salvat, F. (2019), *PENELOPE-2018: A Code System for Monte Carlo Simulation of Electron and Photon Transport*, NEA/OECD, Issy-les-Moulineaux.

Scofield, J. H. (1974), 'Relativistic Hartree-Slater values for K and L X-ray emission rates', *At. Data Nucl. Data Tables* **14**, 121–137.

Seltzer, S. M. (1993), 'Calculation of photon mass energy-transfer and mass energy-absorption coefficients', *Rad. Res.* **136**, 147–170.

Siegbahn, K. (1969), *ESCA Applied to Free Molecules*, North-Holland, Amsterdam.

Simşek, Ö. (2000), 'Differential cross sections for incoherent scattering of γ rays by elements', *Phys. Rev. A* **61**, 042711.

Simşek, Ö., Ertugrul, M., Karabulut, A. & Budak, G. (2002), 'Inelastic scattering of 59.5 keV photons at small momentum transfers by Ti, Fe and Ni elements', *J. Quant. Spect. Rad. Trans.* **75**, 741–746.

Storm, E. & Israel, H. I. (1970), 'Photon cross sections from 1 keV to 100 MeV for elements Z=1 to Z=100', *Nucl. Data Tables* **A7**, 565–681.

Stutz, G. E. (2014), 'Compton scattering cross section for inner-shell electrons in the relativistic impulse approximation', *Nucl. Instrum. Methods B* **319**, 8–16.

Terini, R. A., Nerssissian, D. Y., Campelo, M. C. S., Morice, V. & Yoshimura, E. M. (2020), 'Compton spectrometry applied to clinical CT axial beams from tubes stopped and in revolution', *Radiat. Phys. Chem.* **171**, 108734.

The International Commission on Radiation Units and Measurements (2016), 'Key Data for Ionizing-Radiation Dosimetry, ICRU Report 90', *Journal of the ICRU* **14**(1).

Virtanen, P., Gommers, R., Oliphant, T. E., Haberland, M., Reddy, T., Cournapeau, D., Burovski, E., Peterson, P., Weckesser, W., Bright, J., van der Walt, S. J., Brett, M., Wilson, J., Jarrod Millman, K., Mayorov, N., Nelson, A. R. J., Jones, E., Kern, R., Larson, E., Carey, C. J., Polat, İ., Feng, Y., Moore, E. W., VanderPlas, J., Laxalde, D., Perktold, J., Cimrman, R., Henriksen, I., Quintero, E. A., Harris, C. R., Archibald, A. M., Ribeiro, A. H., Pedregosa, F., van Mulbregt, P. & SciPy 1.0 Contributors (2020), 'SciPy 1.0: fundamental algorithms for scientific computing in Python', *Nature Methods* **17**, 261–272.

Waller, I. & Hartree, D. R. (1929), 'On the intensity of total scattering of X-rays', *Proc. R. Soc. Lond. A* **124**, 119–142.

Woon, D. E. & Dunning Jr, T. H. (1993), 'Gaussian basis sets for use in correlated molecular calculations. III. The atoms aluminum through argon', *J. Chem. Phys.* **98**, 1358–1371.

Yalçin, P. (2002), 'Incoherent scattering of ^{241}[Am] gamma photons', *Spectrochim. Acta B* **57**, 791–796.